Microstructure and Mechanical Properties of Ti-Nb Alloys Prepared by Mechanical Alloying and Spark Plasma Sintering

Damian Kalita, Łukasz Rogal, Tomasz Czeppe, Anna Wójcik, Aleksandra Kolano-Burian, Przemysław Zackiewicz, Bogusz Kania, and Jan Dutkiewicz

The effect of Nb content on microstructure, mechanical properties and superelasticity was studied in Ti-Nb alloys fabricated by powder metallurgy route using mechanical alloying and spark plasma sintering. In the microstructure of the as-sintered materials, undissolved Nb particles as well as precipitations of α-phase at grain boundaries of β-grains were observed. In order to improve the homogeneity of the materials, additional heat treatment at 1250 °C for 24 h was performed. As a result, Nb particles were dissolved in the matrix and the amount of α-phase was reduced to 0.5 vol.%. Yield strength of the as-sintered alloys decreased with Nb content from 949 MPa for Ti-14Nb to 656 MPa for Ti-26Nb, as a result of the decreasing amount of α-phase precipitations. Heat treatment did not have a significant effect on mechanical properties of the alloys. A maximum recoverable strain of 3% was obtained for heat-treated Ti-14Nb, for which A_s and A_f temperatures were − 12.4 and 2.2 °C, respectively.

1. Introduction

Ti-Nb-based alloys are considered as materials for orthopedic implants due to their excellent biocompatibility (Ref 1), low elastic modulus (Ref 2) and good superelastic properties (Ref 3). The superelastic behavior of Ti-Nb alloys is connected with the thermo-elastic martensitic transformation between body-centered cubic (BCC) β parent phase and orthorhombic α'' martensite phase (Ref 3). In the case of pure titanium low-temperature HCP (hexagonal close packed), α-phase transforms to β-phase at 882 °C. However, by adding elements such as Nb, Ta, Mo, the high-temperature β-phase can be stabilized in room temperature (RT) (Ref 4). In binary Ti-Nb system, an addition of 1 at.% of Nb to β-Ti decreases M_s temperature by 40 °C and an addition of 26-27 at.% allows to obtain M_s temperature slightly below room temperature (RT), which ensures optimal RT superelastic properties (Ref 5, 6). Theoret-

ical calculation shows that alloys which contain 26 at.% of Nb maximum strain transformation along [011] direction can reach about 3% (Ref 3). This value can be increased by reducing the concentration of Nb or by replacing Nb by other elements such as Ta, Mo, Zr (Ref 3, 6). The extensive research is focused on shape-memory characteristic of Ti-Nb-based alloys obtained through casting and cold-working processes. For example, Kim et al. (Ref 3) reported a maximum recovery strain of 4.2% in cold-rolled Ti-26Nb alloy aged at 400 °C. Aging of superelastic Ti-Nb alloys is required in order to obtain stable superelastic behavior as a result of the formation of nanometric precipitations of athermal ω-phase which increase critical stress for slip deformation in those alloys (Ref 7, 8). Another way for increasing critical stress for slip deformation is the addition of interstitial elements such as O or N. It was confirmed that an addition of 2 at.% of oxygen to Ti-22Nb increases critical stress for slip deformation up to 890 MPa, but also reduces the maximum recovery strain to about 3% (Ref 9). Nowadays, powder metallurgy (PM) techniques such as mechanical alloying (MA) as well as additive manufacturing (AM) are gaining popularity due to the possibility of fabricating elements with complicated shapes and superior mechanical properties (Ref 10-13).

The powder metallurgy route based on mechanical alloying of pure metal powders followed by consolidation using spark plasma sintering (SPS) is a promising method of preparing a wide range of alloys, in particular when alloying elements have a wide difference in melting points. Moreover, by controlling the processing parameters such as sintering temperature or by introducing space holder materials, porous materials can be obtained, which allow controlling the elastic modulus of the material. Introducing of pore structure to the conventional NiTi SMAs allows obtaining better biocompatibility as a result of reduction in elastic modulus close to the bone values and the ability to grow cells inside the pores (Ref 14). In the case of powder metallurgy processes, the oxygen and nitrogen contaminations have a significant impact on M_s temperature of Ti-

Damian Kalita, Łukasz Rogal, Tomasz Czeppe, Anna Wójcik, Bogusz Kania, and **Jan Dutkiewicz**, Institute of Metallurgy and Materials Science, Polish Academy of Sciences, Reymonta 25 St., 30-059 Kraków, Poland; and **Aleksandra Kolano-Burian** and **Przemysław Zackiewicz**, Institute of Non-Ferrous Metals, Sowinskiego 5 St., 44-100 Gliwice, Poland. Contact e-mail: d.kalita@imim.pl.

Nb-based alloys as well as superelastic properties. It was confirmed that an addition of 1 at.% of O to the Ti-Nb alloys leads to a decrease in M_s temperature by about 160 °C (Ref 15, 16). Similarly, an addition of 1 at.% of N decreases M_s temperature by about 200 °C (Ref 17). This is the reason why the martensitic transformation is not observed in sintered materials even if the Nb content indicates that M_s temperature is close to RT. For example, Lai et al. (Ref 10) show that stable RT superelastic properties can be obtained in binary Ti-Nb alloys prepared by powder metallurgy route by reducing Nb content to about 13%. Yuan et al. (Ref 18) reported high recovery strain of 5.4% in Ti-11Nb alloy containing 4 at.% of oxygen, obtained by mechanical alloying and pressureless sintering. Therefore, in order to obtain superelastic properties in binary Ti-Nb alloys obtained by powder metallurgy route, the Nb concentration has to be reduced to compensate the effect of interstitial atoms on the M_s temperature.

In the presented work, two different compositions of the alloy, containing 14 and 20 at.% of Nb, were chosen based on the typical oxygen content observed in mechanically alloyed Ti-Nb-based alloys, which is in the range 1.0-2.5 at.% (Ref 10, 19, 20). The third alloy containing 26 at.% of Nb was chosen as a reference material in which superelastic behavior is observed in the as-cast state. Because of limited information about the evolution of properties of PM-fabricated Ti-Nb alloys, the aim of the presented work is to analyze the influence of Nb content on the microstructure, mechanical properties and superelastic behavior of Ti-Nb alloys.

2. Experimental

In the presented study, Ti (150 mesh, 99.9%) and Nb (325 mesh, 99.8%) elemental powders, supplied by Alfa Aesar, were used as initial materials. Three different compositions of alloys were prepared using mechanical alloying method—Ti-xNb (where $x = 14$, 20 and 26 at.%). Mechanical alloying was conducted using Fritsch Pulverisette 7 planetary ball mill with rotation speed 150 rpm and cemented tungsten carbide containers and balls. The ball-to-power weight ratio was 10:1. Time of milling was 30 h. In order to avoid extensive oxidation of powders during synthesis, all the operations with powders were conducted in a glovebox under protective argon atmosphere (O_2 and H_2O < 1 ppm). In the next step, powders were consolidated using spark plasma sintering (HP D5/2 FCT System) at 1300 °C for 30 min under 35 MPa pressure in argon atmosphere. Samples 20 mm in diameter and 8 mm high were obtained. Additional annealing at temperature 1250 °C for 24 h was applied in order to improve the homogeneity of sintered samples.

Phase composition of powders and sintered materials was examined using a Philips PW1740 x-ray diffractometer (XRD) using Co-Kα radiation. The lattice constant of β-phase is calculated using Eq 1 (Ref 21):

$$a_\beta = \frac{\lambda \sqrt{h^2 + k^2 + l^2}}{2 \sin \theta} \qquad \text{(Eq 1)}$$

where λ is the wavelength of the x-ray radiation, h, k, and l are Miller indices of the diffraction planes and θ is the Bragg angle. The microstructure of the materials was studied using scanning electron microscopes (SEM) Philips XL-30 and FEI Quanta 3D FEG equipped with EDAX Genesis energy-dispersive x-ray

spectrometer (EDS). More detailed microstructure observations and phase analysis were conducted using a Tecnai G2 F20 transmission electron microscope (TEM). Thin samples for TEM observations were prepared using jet-polisher Struers Tenupol-5 in an electrolyte containing of 10 vol.% of H_2SO_4 in methanol at 10 °C. Differential scanning calorimetry (DSC, Q1000 TA Instruments) was used to characterize phase transformation temperatures of the materials. The temperature range was from − 100 to 100 °C, and the heating/cooling rate was 20 °C/min. Samples for compression test were prepared in the form of cylinders 4 mm in diameter and 6 mm high. Tests were performed using Shimadzu Autograph AG–X plus testing machine at strain rate 10^{-3} 1/s.

3. Results and Discussion

3.1 Powders Characterization After Milling

The XRD patterns of powders, using the Ti-26Nb alloy as an example, at various stages of mechanical alloying are shown in Fig. 1(a). During the synthesis, the amount of hexagonal α-
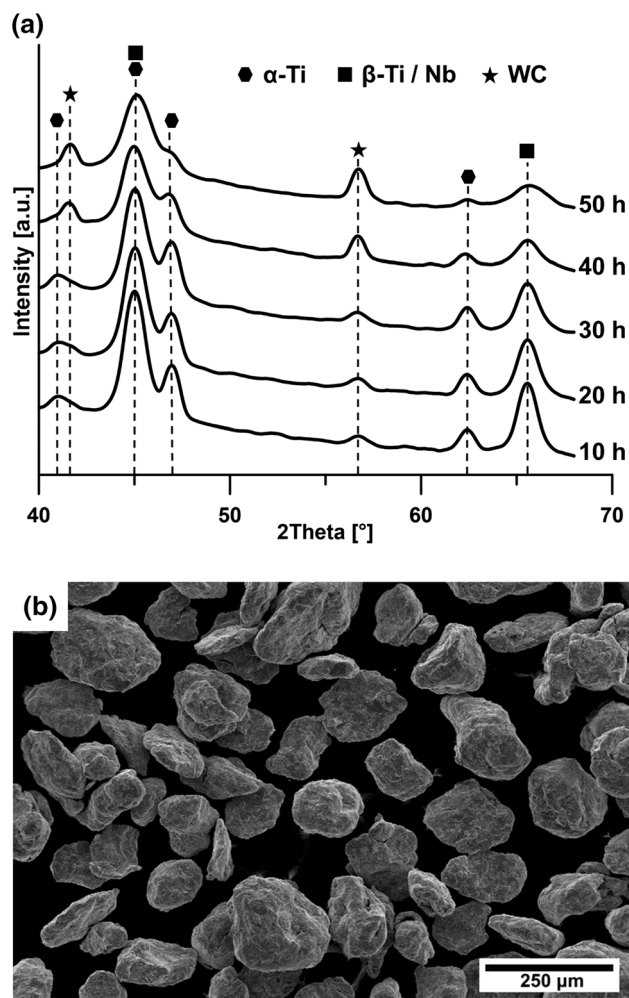

Fig. 1 XRD patterns of powders at various stages of MA (a) and SEM-SE image of the powder after 30 h of MA (b), on example of Ti-26Nb alloy

phase decreases with milling time and after 50 h only trace amount of this phase is observable. β-Ti as well as Nb crystalize in the W-type structure in the space group *Im-3m*, with slight difference in lattice parameters ($a_{β\text{-}Ti}$ = 3.327 Å and a_{Nb} = 3.305 Å); therefore, it is difficult to distinguish them using XRD technique (Ref 22, 23). The observed broadening of peaks during the milling results from the slight deviation of lattice constants connected with severe plastic deformation of powder particles as well as alloying process. It is worth mentioning that, during the synthesis, hexagonal WC phase appears and its amount increases with milling time. The origin of this phase is a result of wear process of cemented tungsten carbide container and milling balls. In order to balance the alloying and wear process, an intermediate time of 30 h was used for powders prepared for sintering. The selected time allows obtaining sufficient level of mixing of the elemental powder and ensures low level of contaminations from the wear process. As shown in Fig. 1(b), the morphology of the obtained powder is close to spherical with average grain size of about 100 µm.

3.2 As-Sintered Alloys

The XRD patterns of the as-sintered materials are shown in Fig. 2. In all alloys, mainly regular β-phase is observed after sintering. Only small amount of hexagonal α-phase is present in the samples. The trace amount of orthorhombic martensite α'' phase is observed in the case of alloys containing 14 and 20 at.% of Nb. It is worth noticing that the WC phase observed in powders after mechanical alloying is not observed in sintered materials. It is possible that WC particles were dissolved in the matrix during sintering (Ref 24). In the microstructure of the obtained alloys, equiaxed β-phase grains with size in range of 10-50 µm are observed, as shown in Fig. 3, in the case of Ti-14Nb alloy. At the grain boundaries, darker areas of α-phase, depleted in Nb, are present. Based on metallographic analysis, as described in (Ref 25), it was determined that the amount of α-phase decreases with Nb content from 2.6 vol.% in the case of Ti-14Nb to 0.9 vol.% for Ti-26Nb. Moreover, very bright areas, containing mainly Nb, are observed, which are attributed to undissolved particles of Nb during sintering. The presence of these particles causes a reduction in Nb content in the matrix. In the case of Ti-14Nb at this stage, the average Nb content in β-grains is 13.3 at.%. Applied sintering conditions allowed to obtain highly dense samples with porosity below 0.5 vol.%.
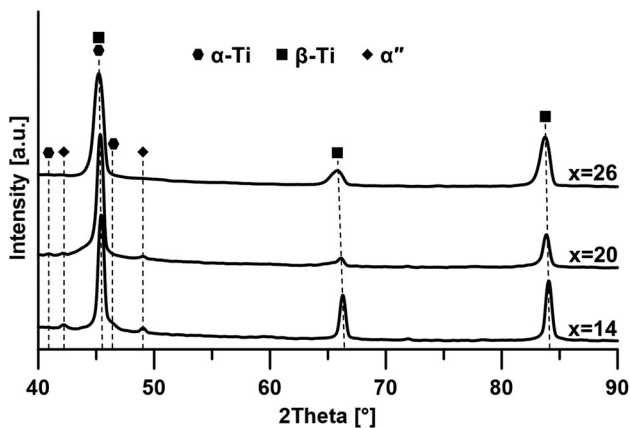
The existence of α-phase at the grain boundaries of β-grains was confirmed using TEM studies (Fig. 4). Bright-field (BF) image shows a thin layer, about 500 nm, of α-phase between two grains of β-phase. The presence of hexagonal α-phase in sintered Ti-Nb alloys was also observed by other authors, even if Nb content in alloys was much higher than the one required to obtain one-phase β-alloys (Ref 11, 26). The α-phase is harder and more brittle in comparison with regular β-phase. For that reason, it is used to increase the mechanical properties of near β-Ti alloys, whereas β-phase maintains good plastic properties, e.g., Ti-10V-2Fe-3Al or Ti-15V-3Cr-3Sn-3Al (Ref 27, 28). In the case of the investigated alloys, α-phase is undesirable, because it can lead to nucleation of cracks at the grain boundaries during deformation, which can reduce the superelastic properties of the alloys. The existence of α-Ti phase and Nb particles is a result of insufficient interdiffusion of Ti and Nb during the sintering process. Therefore, in order to improve the homogeneity of the as-sintered alloys additional heat treatment at temperature of 1250 °C for 24 h was applied.
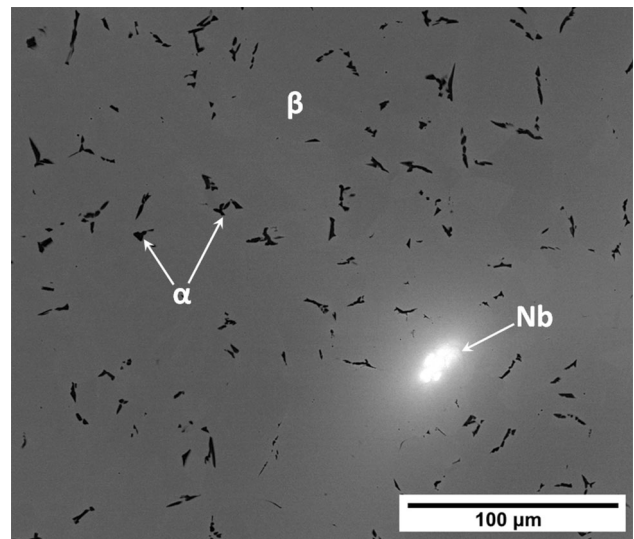

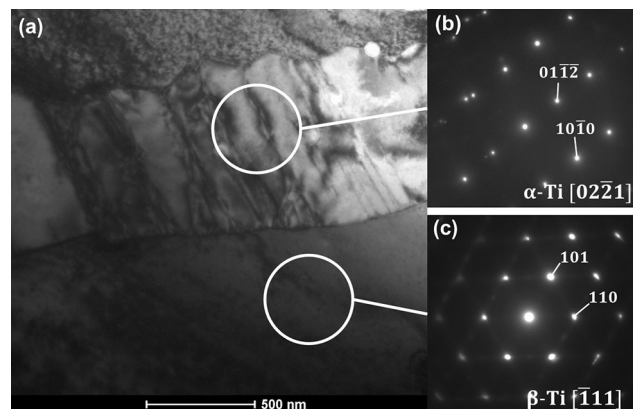**Fig. 3** Typical microstructure of the as-sintered alloys on the example of Ti-14Nb alloy

Fig. 4 TEM-BF image of thin layer of α-phase between two β-phase grains (a) and corresponding SAED patterns (b, c) from areas marked with circles

Fig. 2 XRD patterns of the as-sintered Ti-*x*Nb alloys

3.3 Heat-Treated Alloys

The typical microstructure of heat-treated sample is presented in Fig. 5. Additional annealing leads to increase in homogeneity of the materials. The Nb-rich areas were dissolved in the matrix during this process. As a result, the concentration of Nb in β matrix was increased and reached the value close to initial composition of powders − 14.8 ± 0.3 at.% in the case of Ti-14Nb alloy, 20.5 ± 0.6 at.% for Ti-20Nb and 26.7 ± 0.3 at.% for Ti-26Nb. In addition, slight grain growth of β-phase was observed. Annealing leads to the change in morphology of the α-phase from precipitations at the grain boundaries (Fig. 3) to colony of isolated α-grains–darker grains in Fig. 5. The amount of the α-phase was reduced to about 0.5 vol.% in the case of all materials. Hexagonal α-phase could not be completely dissolved in the matrix during the high-temperature annealing due to presence of contaminations. It was confirmed, using EDS technique, that the concentration of carbon in α-phase areas is much higher in comparison with β-phase areas. It is well known that carbon highly stabilizes α-phase, therefore the α-phase areas can exist even after 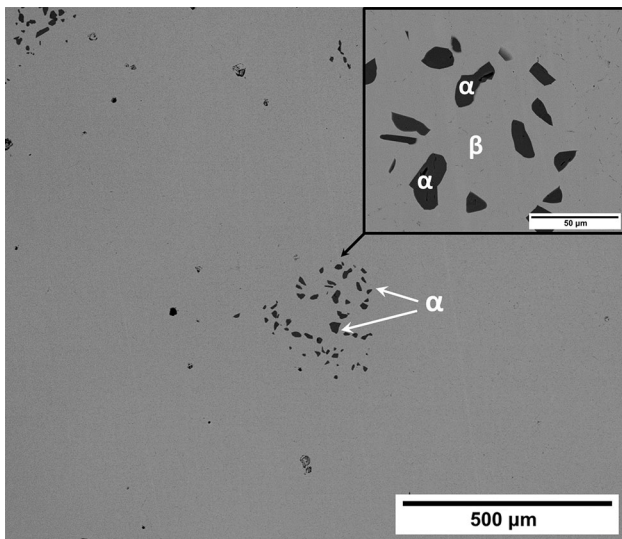long-term annealing (Ref 29). Carbon is observed in obtained materials as a result of dissolution of the WC particles, observed in powder before sintering (Fig. 1a), and come from wear process of reactor and milling balls during mechanical alloying. Chemical analysis of the matrix shows that it contains

Fig. 5 Typical microstructure of heat-treated alloys on the example of Ti-14Nb alloy
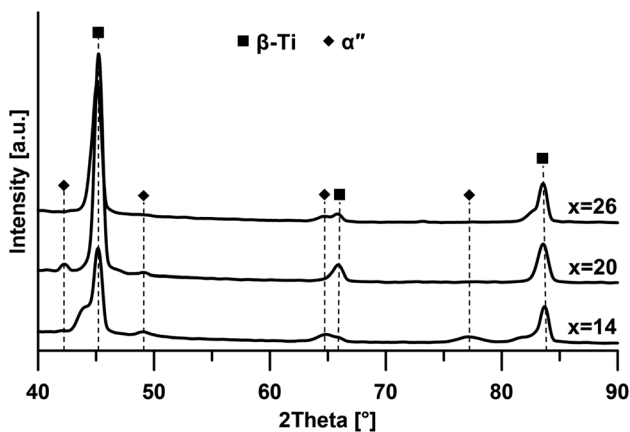
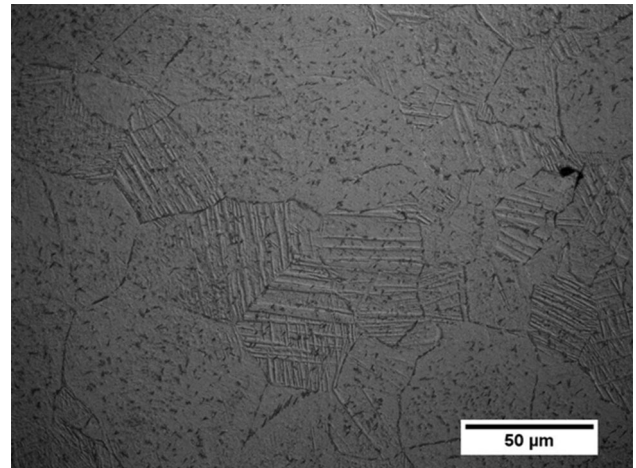Fig. 6 XRD patterns of heat-treated Ti-xNb alloys

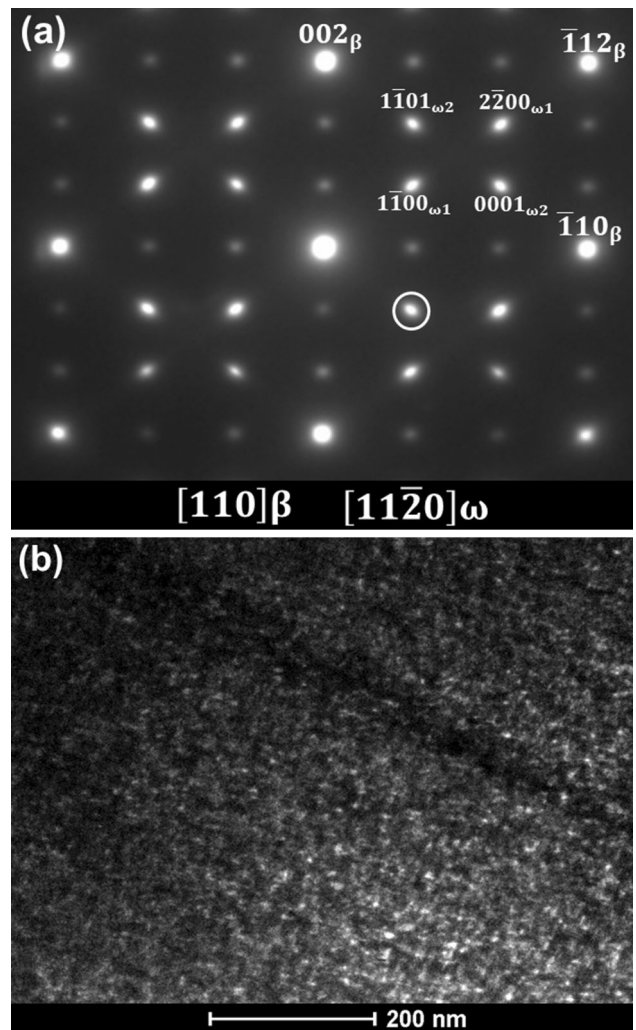Fig. 7 OM microstructure of Ti-14Nb alloy after heat treatment

Fig. 8 SAED pattern (a) and corresponding DF TEM image (b) of heat-treated Ti-14Nb alloy

about 1 at.% of W which confirms that the WC particles were dissolved during the sintering. At this stage, the measured porosity was 0.5 vol.% in the case of all materials, similar to the materials in the as-sintered condition.

The phase analysis, shown in Fig. 6, confirms that the applied heat treatment resulted in a reduced amount of hexagonal α-phase—peaks connected with α-phase are not observed after heat treatment. In all of the alloys, regular β-phase is observed. The lattice parameter of β-phase, calculated based on Eq 1, is 2.325 Å for Ti-14Nb, 2.326 Å for Ti-20Nb and 2.325 Å for Ti-26Nb alloy, which is in good agreement with others research (Ref 3). However, in the case of Ti-20Nb and Ti-14Nb martensitic transformation has taken place during cooling after heat treatment. This observation was also confirmed by microscopic observation. Figure 7 shows an optical microscopy (OM) image of the microstructure of the heat-treated Ti-14Nb alloy etched by Kroll's reagent. In the microstructure of these alloys, a martensitic phase exceptionally can be observed inside grains of β-phase, which suggest that M_s temperature of this alloy is close to RT.

TEM observations of heat-treated alloys, similar to the as-sintered materials, reveal the existence of nanoprecipitations of the hexagonal ω-phase. There are two types of ω-phase in titanium alloys—thermal ω-phase which is formed during aging at intermediate temperatures and athermal ω-phase which is observed in solution-treated alloys (Ref 30, 31). Both of these phases affect the properties of titanium alloys, e.g., an increase in the hardness from 200 HV to 440 HV during annealing of Ti-30Nb alloy was observed, as a result of thermal ω-phase formation (Ref 2). Because of the formation process of the ω-phase, described in more details in (Ref 32), there are four different variants of ω-phase, which have the orientation relationship with the parent β-phase as follows: $\{0001\}_\omega$//$\{111\}_\beta$ (Ref 11-20) $_\omega$//$[110]_\beta$ (Ref 3). Figure 8 shows dark-field (DF) TEM image and corresponding SAED pattern of heat-treated Ti-14Nb alloy. The SAED pattern was obtained from the $[110]_\beta$ zone axis. In addition to the primary reflections from the β matrix, diffused scattering corresponding with the athermal ω-phase at $^1/_3$ $\{112\}_\beta$ positions was observed. DF image obtained using ω-phase reflection, marked by circle in Fig. 8(a), indicates that ω-phase in the investigated alloys appears in the form of nanometric precipitations, uniformly distributed in the β-phase matrix. The presence of ω-phase in Ti-Nb alloys was also described by other authors (Ref 33, 34). The dispersed ω-particles increase the strength of the alloys, but on the other hand mechanically suppress the martensitic
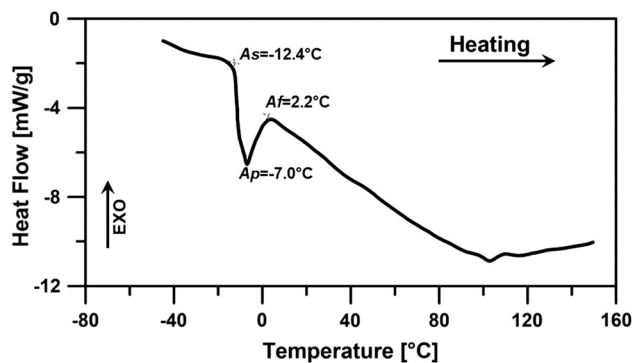
transformation, resulting in a decrease in the martensitic transformation temperature (Ref 3).

Thermal analysis was carried out in order to determine the temperature range of reversible β↔α″ martensitic transformation in investigated alloys. Figure 9 show the DSC heating curve of the Ti-14Nb alloy after heat treatment. Determined for this alloy A_s and A_f temperatures are − 12.4 and 2.2 °C, respectively. These values are in agreement with other works, e.g., Lai et al. (Ref 10) showed martensitic transformation in the temperature about 0 °C in sintered Ti-14Nb alloy. Although the A_s temperature for this composition lies below RT, α″ martensite can be observed in the microstructure of the alloy (Fig. 6 and 7) as a result of possible residual stresses after heat treatment. There were no observable effects connected with martensitic transformation in the case of alloys containing 20 and 26 at.% of Nb in the temperature range from − 100 to 100 °C. It is probable that for these alloys, temperature range of
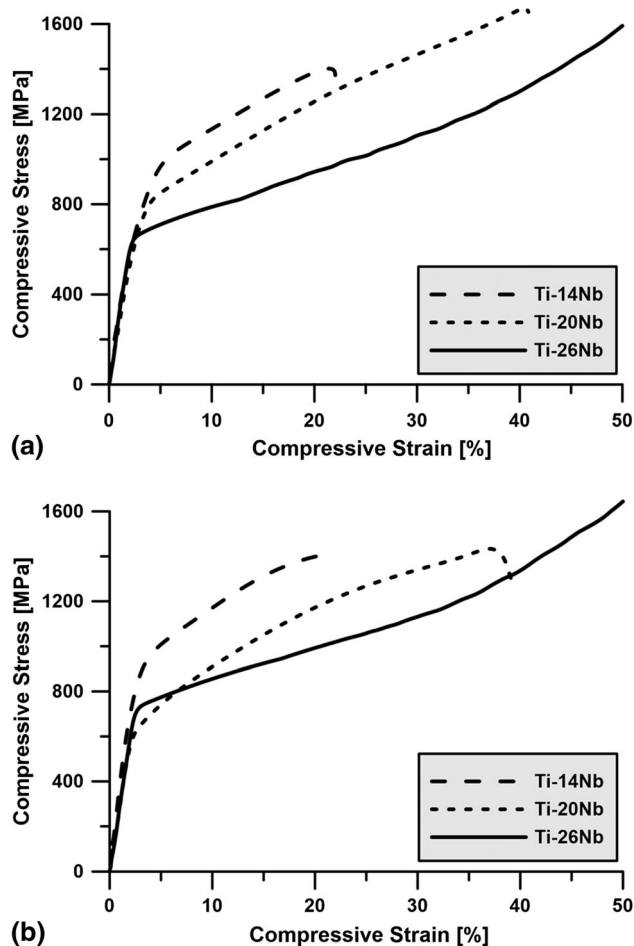

(a)

(b)

Fig. 10 Compressive stress–strain curves of Ti-xNb alloys in the as-sintered (a) and heat-treated (b) states

Table 1 Mechanical properties of investigated alloys

	Yield strength, MPa		
	Ti-14Nb	**Ti-20Nb**	**Ti-26Nb**
As-sintered	949 ± 36	746 ± 19	656 ± 10
Heat-treated	921 ± 30	624 ± 26	710 ± 14

Fig. 9 DSC heating curve of heat-treated Ti-14Nb alloy

martensitic transformation lies much below RT. For example, M_s temperature for sintered Ti-18Nb was extrapolated to about − 160 °C (Ref 10).

3.4 Mechanical Properties

The compression tests were carried out in order to determine the mechanical properties of obtained alloys. Compression curves of the as-sintered alloys, presented in Fig. 10(a), show that yield strength (YS) of the investigated alloys, listed in Table 1, decreases with Nb content. On the other hand, compressive strain increases with Nb content and in the case of alloy containing 26 at.% of Nb exceeds 50%. This dependence is connected with the presence of hexagonal α-phase in the microstructure of the as-sintered materials, as described in paragraph 3.2. With increasing Nb concentration, the amount of the α-phase decreases and as a result the YS decreases and the plasticity increases.

Figure 10(b) shows compressive curves of heat-treated materials. Although the applied heat treatment leads to an increase in the homogeneity of the materials, only small changes in mechanical properties were observed. In the case of alloys containing 14 and 20 at.% of Nb, a slight decrease in YS was noted. On the other hand, for Ti-26Nb alloy, the YS increased by about 50 MPa. No changes were observed in compression strain. Slight difference in the mechanical properties between the as-sintered and heat-treated materials can be attributed to a few processes taking place during the annealing. First of all, annealing leads to grain growth, which can reduce the properties of the alloys, as described by the Hall–Petch relationship. Simultaneously, the reduction in amount of hexagonal α-phase precipitations, as well as, undissolved Nb particles, which also had influence on mechanical properties, was observed. On the other hand, the formation of nanometric precipitations of ω-phase during high-temperature annealing leads to an increase in mechanical properties (Ref 8). It is important to note that Ti-Nb alloys obtained by casting techniques exhibit much lower mechanical properties in comparison with obtained alloys. YS of casted and solution-treated alloys typically did not excess 400 MPa (Ref 8, 35), whereas this value for alloys obtained by powder metallurgy route typically exceeded 1000 MPa (Ref 19, 36). There are several possible reasons describing the increased mechanical properties of alloy obtained by powder metallurgy route in comparison with cast alloys. First of all, the oxygen and nitrogen contaminations caused the solution-hardening effect, which increases mechanical properties of the alloy, e.g., addition of 2 at.% of oxygen to Ti-22Nb alloy increases the fracture stress of the alloy to 1.37 GPa (Ref 9). Secondly, the observed α-phase precipitations in fabricated alloys also lead to an increase in the mechanical properties, as in the case of near-β Ti alloys (Ref 27). The frequently observed, in the case of mechanically alloyed materials, nanoparticles of oxides also can increase the properties of the materials (Ref 37).

In order to determine the superelastic properties of the investigated alloys, cyclic compression tests were carried out. At the first cycle, compressive strain reached 1% and then the stress was removed. The tests were repeated, for the same sample, by increasing strain by 0.5%, for every cycle, up to 5%. Test was carried out at room temperature. The maximum recoverable strain as high as 3% was obtained in the case of Ti-14Nb alloy, as shown in Fig. 11. Recoverable strain for alloys with 20 and 26 at.% of Nb was 2.2 and 1.9%, respectively.
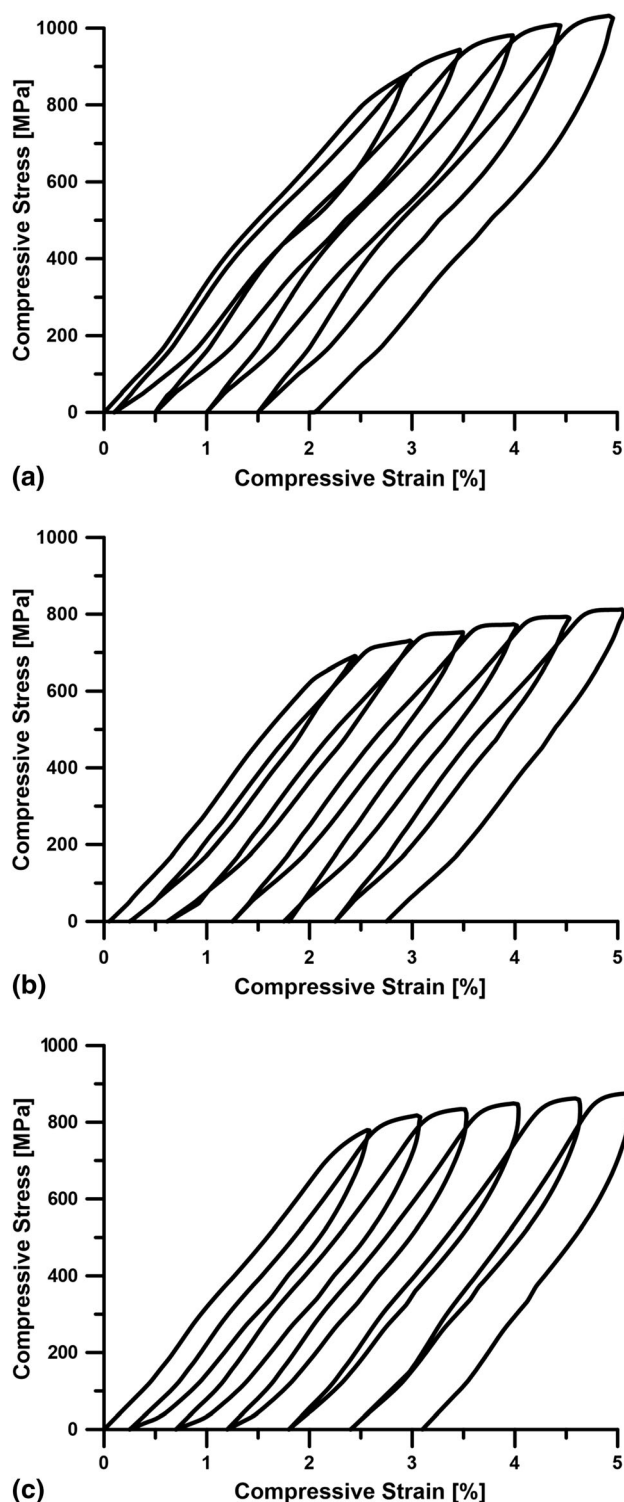

Fig. 11 Compressive stress–strain curves obtained by cyclic loading–unloading test of the heat-treated Ti-14Nb (a), Ti-20Nb (b) and Ti-26Nb (c)

Total recoverable strain is composed of three parts: the recovery of its own elasticity (R_E), the elastic recovery of pore structure (R_P) and recovery connected with reversible martensitic transformation (R_{MT}) (Ref 10). The porosity of fabricated materials is low (does not exceed 0.2%), therefore R_P part can be neglected. In the case of Ti-20Nb and Ti-26Nb alloys, A_s

and A_f are far away from the room temperature, and hence the determined recovery strain is connected mainly with the R_E part. It is well known that the elasticity of the β-phase Ti alloys is generally high when it contains an elevated amount of oxygen (Ref 38, 39). The superelastic behavior was observed only for alloy containing 14 at.% of Nb. DSC measurements show that A_s and A_f temperatures, of this alloy, are slightly below room temperature, which should provide the optimal superelastic properties. The obtained value is close to the superelasticity of solution-treated alloys fabricated by casting methods, e.g., Kim et al. (Ref 3) reported a maximum recovery strain of 2.5% in cold-rolled and solution-treated Ti-26Nb alloy; however, the R_E in the case of alloys obtained by powder metallurgy techniques is much higher in comparison with cast alloys, because of low critical stress for slip deformation in the case of cast alloys.

4. Conclusions

In order to determine the influence of Nb content on the microstructure, mechanical properties and superelastic behavior of β-type Ti-Nb alloys, mechanical alloying followed by spark plasma sintering techniques were used to prepare Ti-xNb (where $x = 26, 20, 14$) alloys. The obtained results are as follows:

(1) The applied sintering conditions (temperature 1300 °C, pressure 35 MPa, time 30 min) allow to obtain dense samples, with porosity below 0.5 vol.%; however, additional annealing at 1250 °C for 24 h had to be applied in order to increase the homogeneity of the as-sintered materials. As a result, the concentration of Nb in the matrix reached the value close to the intended, and amount of hexagonal α-phase was reduced to about 0.5 vol.%.

(2) Mechanical properties of fabricated alloys are higher in comparison with cast Ti-Nb alloys. YS of the as-sintered alloys decreases with Nb content from 950 MPa for Ti-14Nb to 650 MPa for Ti-26Nb, as a result of decrease in the volume fraction of α-phase with Nb content. Heat treatment has no significant effect on mechanical properties of the alloys.

(3) Superelastic behavior at RT was observed for heat-treated Ti-14 alloy. This alloy exhibited maximum recoverable strain up to 3%. Determined for this alloy, by DSC technique, A_s and A_f temperatures were -12.4 and 2.2 °C, respectively.

Open Access

References

1. B.L. Wang, L. Li, and Y.F. Zheng, In Vitro Cytotoxicity and Hemocompatibility Studies of Ti-Nb, Ti-Nb-Zr and Ti-Nb-Hf Biomedical Shape Memory Alloys, *Biomed. Mater.*, 2010, **5**(4), p 04410
2. E.S.N. Lopes, A. Cremasco, C.R.M. Afonso, and R. Caram Lopes, Effects of Double Aging Heat Treatment on the Microstructure, Vickers Hardness and Elastic Modulus of Ti-Nb Alloys, *Mater. Charact.*, 2011, **62**(7), p 673–680
3. H.Y. Kim, Y. Ikehara, J.I. Kim, H. Hosoda, and S. Miyazaki, Martensitic Transformation, Shape Memory Effect and Superelasticity of Ti-Nb Binary Alloys, *Acta Mater.*, 2006, **54**(9), p 2419–2429
4. D. Kuroda, M. Niinomi, M. Morinaga, Y. Kato, and T. Yashiro, Design and Mechanical Properties of New β Type Titanium Alloys for Implant Materials, *Mater. Sci. Eng. A*, 1998, **243**(1-2), p 244–249
5. H.Y. Kim, S. Hashimoto, J.I. Kim, H. Hosoda, and S. Miyazaki, Mechanical Properties and Shape Memory Behavior of Ti-Nb Alloys, *Mater. Trans.*, 2004, **45**(7), p 2443–2448
6. H.Y. Kim and S. Miyazaki, Several Issues in the Development of Ti-Nb-Based Shape Memory Alloys, *Shape Mem. Superelast.*, 2016, **2**(4), p 380–390
7. A. Cremasco, P.N. Andrade, R.J. Contieri, E.S.N. Lopes, C.R.M. Afonso, and R. Caram, Correlations Between Aging Heat Treatment, ω Phase Precipitation and Mechanical Properties of a Cast Ti-Nb Alloy, *Mater. Des.*, 2011, **32**(4), p 2387–2390
8. H.Y. Kim, J.I. Kim, T. Inamura, H. Hosoda, and S. Miyazaki, Effect of Thermo-mechanical Treatment on Mechanical Properties and Shape Memory Behavior of Ti-(26-28) at.% Nb Alloys, *Mater. Sci. Eng. A*, 2006, **438**, p 839–843
9. J.I. Kim, H.Y. Kim, H. Hosoda, and S. Miyazaki, Shape Memory Behavior of Ti-22Nb-(0.5-2.0) O (at%) Biomedical Alloys, *Mater. Trans.*, 2005, **46**(4), p 852–857
10. M. Lai, Y. Gao, B. Yuan, and M. Zhu, Remarkable Superelasticity of Sintered Ti-Nb Alloys by M_s Adjustment Via Oxygen Regulation, *Mater. Des.*, 2015, **87**, p 466–472
11. B. Sharma, S.K. Vajpai, and K. Ameyama, Microstructure and Properties of Beta Ti-Nb Alloy Prepared by Powder Metallurgy Route Using Titanium Hydride Powder, *J. Alloys Compd.*, 2016, **656**, p 978–986
12. Y.J. Liu, Y.S. Zhang, and L.C. Zhang, Transformation-Induced Plasticity and High Strength in Beta Titanium Alloy Manufactured by Selective Laser Melting, *Materialia*, 2019, **6**, p 100299
13. J.C. Wang, Y.J. Liu, P. Qin, S.X. Liang, T.B. Sercombe, and L.C. Zhang, Selective Laser Melting of Ti-35Nb Composite from Elemental Powder Mixture: Microstructure, Mechanical Behavior and Corrosion Behavior, *Mater. Sci. Eng., A*, 2019, **760**, p 214–224
14. S. Kujala, J. Ryhänen, A. Danilov, and J. Tuukkanen, Effect of Porosity on the Osteointegration and Bone Ingrowth of a Weight-Bearing Nickel-Titanium Bone Graft Substitute, *Biomaterials*, 2003, **24**(25), p 4691–4697
15. M. Tahara, H.Y. Kim, T. Inamura, H. Hosoda, and S. Miyazaki, Lattice Modulation and Superelasticity in Oxygen-Added β-Ti Alloys, *Acta Mater.*, 2011, **59**(16), p 6208–6218
16. S. Miyazaki, H.Y. Kim, and H. Hosoda, Development and Characterization of Ni-Free Ti-Base Shape Memory and Superelastic Alloys, *Mater. Sci. Eng. A*, 2006, **438**, p 18–24
17. M. Tahara, H.Y. Kim, H. Hosoda, and S. Miyazaki, Shape Memory Effect and Cyclic Deformation Behavior of Ti-Nb-N Alloys, *Funct. Mater. Lett.*, 2009, **2**(02), p 79–82
18. B. Yuan, B. Yang, Y. Gao, M. Lai, X.H. Chen, and M. Zhu, Achieving Ultra-High Superelasticity and Cyclic Stability of Biomedical Ti-11Nb-4O (at.%) Alloys by Controlling Nb and Oxygen Content, *Mater. Des.*, 2016, **92**, p 978–982

19. L.M. Zou, C. Yang, Y. Long, Z.Y. Xiao, and Y.Y. Li, Fabrication of Biomedical Ti-35Nb-7Zr-5Ta Alloys by Mechanical Alloying and Spark Plasma Sintering, *Powder Metall.*, 2012, **55**(1), p 65–70

20. J. Málek, F. Hnilica, J. Veselý, and B. Smola, Heat Treatment and Mechanical Properties of Powder Metallurgy Processed Ti-35.5 Nb-57Ta Beta-Titanium Alloy, *Mater. Charact.*, 2013, **84**, p 225–231

21. B.D. Cullity, S.R. Stock, *Elements of X-Ray Diffraction*, Vol 3, Prentice Hall, New Jersey, 2001

22. T.B. Massalski, *Binary Alloy Phase Diagrams*, Vol 2, American Society for Metals, Cleveland, 1986

23. C. Salvo, C. Aguilar, R. Cardoso-Gil, A. Medina, L. Bejar, and R.V. Mangalaraja, Study on the Microstructural Evolution of Ti-Nb Based Alloy Obtained by High-Energy Ball Milling, *J. Alloys Compd.*, 2017, **720**, p 254–263

24. D. Liu, P. Hu, and G. Min, Interfacial Reaction in Cast WC Particulate Reinforced Titanium Metal Matrix Composites Coating Produced by Laser Processing, *Opt. Laser Technol.*, 2015, **69**, p 180–186

25. C.D. Rabadia, Y.J. Liu, S.F. Jawed, L. Wang, Y.H. Li, X.H. Zhang, T.B. Sercombe, H. Sun, and L.C. Zhang, Improved Deformation Behavior in Ti-Zr-Fe-Mn Alloys Comprising the C14 Type Laves and β Phases, *Mater. Des.*, 2018, **160**, p 1059–1070

26. R. Karre, B.K. Kodli, A. Rajendran, J. Nivedhitha, D.K. Pattanayak, K. Ameyama, and S.R. Dey, Comparative Study on Ti-Nb Binary Alloys Fabricated Through Spark Plasma Sintering and Conventional P/M Routes for Biomedical Application, *Mater. Sci. Eng. C*, 2019, **94**, p 619–627

27. I. Weiss and S.L. Semiatin, Thermomechanical Processing of Beta Titanium Alloys—An Overview, *Mater. Sci. Eng. A*, 1998, **243**(1-2), p 46–65

28. S. Shekhar, R. Sarkar, S.K. Kar, and A. Bhattacharjee, Effect of Solution Treatment and Aging on Microstructure and Tensile Properties of High Strength β Titanium Alloy, Ti-5Al-5V-5Mo-3Cr, *Mater. Des.*, 2015, **66**, p 596–610

29. M.J. Donachie, *Titanium: A Technical Guide*, Cleveland, ASM International, 2000, p 13–21

30. J.J.G. Moreno, M. Bönisch, N.T. Panagiotopoulos, M. Calin, D.G. Papageorgiou, A. Gebert, J. Eckert, G.A. Evangelakis, and C.E. Lekka, Ab-Initio and Experimental Study of Phase Stability of Ti-Nb Alloys, *J. Alloys Compd.*, 2017, **696**, p 481–489

31. Y.F. Xu, D.Q. Yi, H.Q. Liu, B. Wang, and F.L. Yang, Age-Hardening Behavior, Microstructural Evolution and Grain Growth Kinetics of Isothermal ω Phase of Ti-Nb-Ta-Zr-Fe Alloy for Biomedical Applications, *Mater. Sci. Eng. A*, 2011, **529**, p 326–334

32. S. Miyazaki, My Experience with Ti-Ni-Based and Ti-Based Shape Memory Alloys, *Shape Mem. Superelast.*, 2017, **3**(4), p 279–314

33. M.J. Lai, C.C. Tasan, J. Zhang, B. Grabowski, L.F. Huang, and D. Raabe, Origin of Shear Induced β to ω Transition in Ti-Nb-Based Alloys, *Acta Mater.*, 2015, **92**, p 55–63

34. D.L. Moffat and D.C. Larbalestier, The Competition Between Martensite and Omega in Quenched Ti-Nb Alloys, *Metall. Trans. A*, 1988, **19**(7), p 1677–1686

35. H.Y. Kim, J. Fu, H. Tobe, J.I. Kim, and S. Miyazaki, Crystal Structure, Transformation Strain, and Superelastic Property of Ti-Nb-Zr and Ti-Nb-Ta Alloys, *Shape Mem. Superelast.*, 2015, **1**(2), p 107–116

36. M. Lai, Y. Gao, B. Yuan, and M. Zhu, Indirect Determination of Martensitic Transformation Temperature of Sintered Nickel-Free Ti-22Nb-6Zr Alloy by Low Temperature Compression Test, *Mater. Des.*, 2014, **60**, p 193–197

37. Y. Long, H. Zhang, T. Wang, X. Huang, Y. Li, J. Wu, H. Chen, and L. Yan, High-Strength Ti-6Al-4V with Ultrafine-Grained Structure Fabricated by High Energy Ball Milling and Spark Plasma Sintering, *Mater. Sci. Eng. A*, 2013, **585**, p 408–414

38. P. Castany, A. Ramarolahy, F. Prima, P. Laheurte, C. Curfs, and T. Gloriant, In Situ Synchrotron X-Ray Diffraction Study of the Martensitic Transformation in Superelastic Ti-24Nb-0.5N and Ti-24Nb-0.5 O Alloys, *Acta Mater.*, 2015, **88**, p 102–111

39. Q. Wei, L. Wang, Y. Fu, J. Qin, W. Lu, and D. Zhang, Influence of Oxygen Content on Microstructure and Mechanical Properties of Ti-Nb-Ta-Zr Alloy, *Mater. Des.*, 2011, **32**(5), p 2934–2939